Macromolecules

Article

pubs.acs.org/Macromolecules

Terms of Use CC-BY

Benzotrithiophene Copolymers: Influence of Molecular Packing and Energy Levels on Charge Carrier Mobility

Bob C. Schroeder,*,† Stephan Rossbauer,‡ R. Joseph Kline,§ Laure Biniek,† Scott E. Watkins,∥ Thomas D. Anthopoulos,‡ Iain McCulloch,† and Christian B. Nielsen†

†Department of Chemistry and Centre for Plastic Electronics, Imperial College London, London SW7 2AZ, U.K.

‡Department of Physics and Centre for Plastic Electronics, Imperial College London, London SW7 2AZ, U.K.

§Material Science and Engineering Division, National Institute of Standards and Technology (NIST), Gaithersburg, Maryland 20899, United States

∥CSIRO Materials Science and Engineering, Melbourne, VIC 3169, Australia

Supporting Information

ABSTRACT: The planar benzotrithiophene unit (**BTT**) was incorporated into four different donor polymers, and by systematically changing the nature and positioning of the solubilizing alkyl side chains along the conjugated backbone, the polymers' frontier energy levels and optoelectronic properties were controlled. Reducing the steric hindrance along the polymer backbone lead to strong interchain aggregation and highly ordered thin films, achieving hole mobilities of 0.04 cm^2/(V s) in organic thin film transistors. In an attempt to increase the polymer's processability and reduce chain aggregation, steric hindrance between alkyl side chains was exploited. As a result of the increased solubility, the film forming properties of the polymer could be improved, but at the cost of reduced hole mobilities in OFET devices, due to the lack of long-range order in the polymer films.

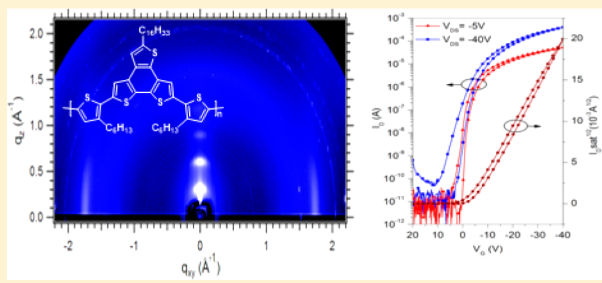

■ INTRODUCTION

Silicon is one of the most common semiconductors used in the fabrication of electronic components, despite the high production costs of electronic grade silicon and its very brittle character. Cheaper and more versatile semiconductors based on organic materials are poised to enter the market, especially for applications requiring flexible substrates and low manufacturing costs (i.e., thin flexible displays, one-way electronics, radio-frequency identification tags, etc.).[1] However, to gain market share over inorganic silicon, it will not be enough for organic semiconductors to be compatible with flexible substrates and cheaper in production than silicon, but they will have to achieve comparable electronic properties, notably similar carrier mobilities (~1 cm^2/(V s) for amorphous silicon) and lifetimes. Extensive work has been done in recent years to investigate how the molecular structure of semiconducting polymers influences the charge carrier mobility and what parameters can be modified to enhance device lifetime and processability.[2−9]

Herein we present a series of benzotrithiophene (**BTT**)-based donor copolymers (Scheme 1), on which electron-withdrawing carbonyl groups have been introduced to the polymer backbone to modulate the polymer's frontier energy levels, thus allowing us to investigate the effects on charge carrier mobilities and device lifetimes. However, the carbonyl groups not only influence the electronic structure of the materials but also have a significant influence on the molecular packing and the solubility of the polymers; therefore, a second set of polymers with head-to-head alkyl chain arrangement was synthesized to increase solubility in organic solvents.

■ RESULTS AND DISCUSSION

The **BTT** moieties were synthesized according to our previously published synthetic pathways.[10,11] To favor intermolecular packing of the **BTT** cores, we decided to attach long linear hexadecyl and hexadecanoyl side chains. The electron-withdrawing character of the acyl side chain perturbs the electron distribution of the **BTT** core compared to the alkyl side chain, as depicted in Figure 1. In contrast to the alkylated **BTT**, the HOMO of the acylated **BTT** (**COBTT**) is no longer distributed over the entire **BTT** core but splits up into a delocalized wave function on the lower benzodithiophene unit and a second more localized wave function on the upper thiophene, to which the carbonyl group is attached. In addition, a significant portion of the lowest unoccupied molecular orbital (LUMO) is located on the carbonyl group of the **COBTT** unit, whereas in the case of the **BTT** moiety, the LUMO is mainly located on the **BTT** core and not on the attached alkyl chain.

Received: January 21, 2014
Revised: April 3, 2014
Published: April 15, 2014

 © 2014 American Chemical Society

Scheme 1. Synthetic Route toward the Extended BTT Monomers

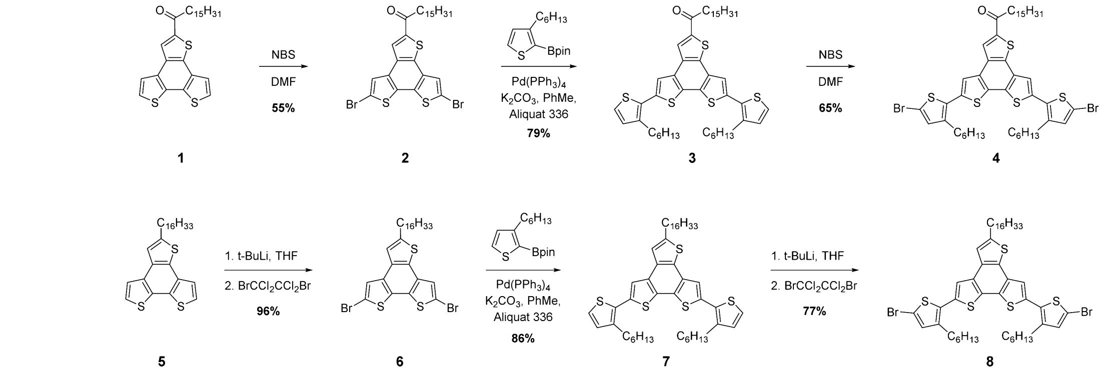

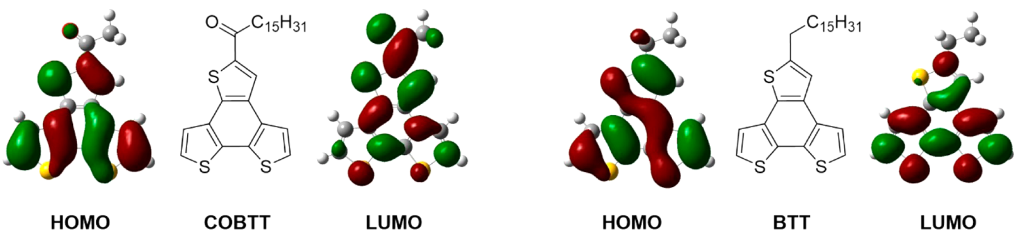

Figure 1. Energy-minimized structure (B3LYP/6-31G*) of methyl-substituted **COBTT** and **BTT** with visualizations of the HOMO and LUMO wave functions, respectively.

Scheme 2. Synthesis of the BTT Polymers

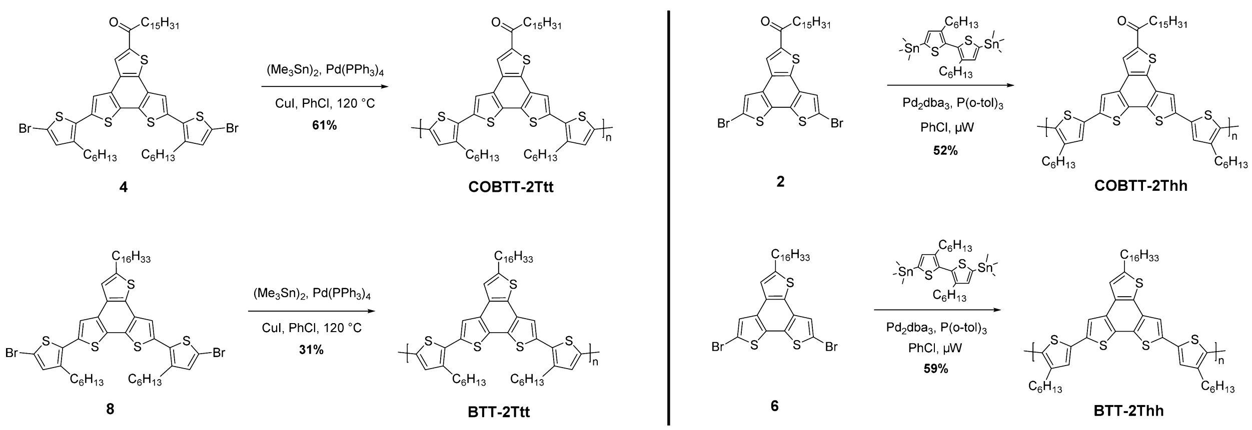

Besides modifying the frontier energy levels of **BTT** copolymers, we were interested in tuning the processability as well. The positioning and the steric hindrance caused by the addition of alkyl chains will determine solubility and molecular packing.[12] In this study we combined both **BTT** donor moieties with either 4,4′-dihexyl-2,2′-bithiophene, which introduces a tail-to-tail (**tt**) or 5,5′ coupling between two adjacent thiophene rings, or with 3,3′-dihexyl-2,2′-bithiophene, causing a head-to-head (**hh**) or 2,2′ coupling.

By extending our previously published synthetic route, a range of brominated **BTT** monomers were easily accessible (Scheme 1).[10,11] Whereas the dibromination with *N*-bromosuccinimide proceeds smoothly in the case of the acylated **BTT** (**1**) at the *α*-positions, we have previously found the electrophilic substitution to be more difficult at these positions in the case of the alkylated **BTT** (**5**), and the bromination conditions needed to be adjusted to achieve a higher selectivity. After Suzuki–Miyaura coupling with 2-(3-hexylthiophen-2-yl)boronic acid pinacol ester and subsequent bromination, the final monomers **4** and **8** were obtained in good purities and high yields. Both monomers were homopolymerized in the presence of hexamethylditin and tetrakis(triphenylphosphine)palladium(0) to yield polymers **COBTT-2Ttt** and **BTT-2Ttt**, respectively.[13] Polymers **COBTT-2Thh** and **BTT-2Thh** were synthesized by copolymerizing compounds **2** and **6**, respectively, with (3,3′-dihexyl-2,2′-bithiophene-5,5′-diyl)bis(trimethylstannane) (Scheme 2).

All four polymers were end-capped after successful polymerization with phenyl end-groups to ensure the removal of reactive trimethyltin or bromide groups, which have been shown to cause charge trapping in organic field effect transistors.[14] It is noteworthy that because of the non-centrosymmetric nature of the different **BTT** monomers, the synthesized polymers should be regiorandom in nature. After precipitation in methanol, the crude polymers were purified by Soxhlet extraction; the chloroform fractions, or chlorobenzene fraction in the case of **BTT-2Ttt**, were washed with an aqueous solution of sodium diethyldithiocarbamate to remove residual palladium.[15] Because of the high tendency of some of the tail–tail polymers to aggregate in solution, gel permeation chromatography (GPC) was performed at 140 °C in 1,2,4-trichlorobenzene, and the results are summarized in Table 1.

Table 1. Molecular Weights and Thermal Stability of the Various BTT Copolymers

polymer	M_n[a] (kg/mol)	M_w[b] (kg/mol)	$Đ_w$[c]	T_d[d] (°C)
COBTT-2Ttt	N.A.	N.A.	N.A.	460
BTT-2Ttt	18	26	1.4	450
COBTT-2Thh	23	55	2.4	460
BTT-2Thh	44	58	1.3	470

[a]Number-average molecular weight. [b]Weight-average molecular weight. [c]Weight-average dispersity M_w/M_n. [d]Decomposition temperature (5% weight loss) determined by thermal gravimetric analysis under nitrogen.

COBTT-2Ttt was observed to aggregate in solution, and even though the GPC traces were recorded at 140 °C, the aggregation could not be overcome and the molecular weight determination was unsuccessful. All other polymers were synthesized with good molecular weights and reasonable dispersities. Thermal gravimetric analysis revealed the exceptional thermal stability of all polymers, and the lowest decomposition temperature was observed for **BTT-2Ttt** at around 450 °C.

We observed significant differences between the solution and solid-state UV–vis absorption spectra, depending on the alkyl side chain attachment (see Figure 2). In the case of a head-to-head coupling between adjacent thiophene rings, a significant backbone twist reduces electron delocalization, and thus the spectra of **COBTT-2Thh** and **BTT-2Thh** are hypsochromically shifted compared to their tail-to-tail coupled counterparts. **BTT-2Thh** presents the most blue-shifted absorption peaks in solution and solid state of all studied polymers. In the solid state, the absorption peak is only slightly red-shifted but significantly broadened (~40 nm) compared to the solution spectrum (Table 2). The similarity of the solution and solid state spectra and the lack of vibronic features in the latter are indicative that the **BTT-2Thh** polymer does not exhibit a strong tendency to order, which is reflected in the polymer's excellent solubility and processability.

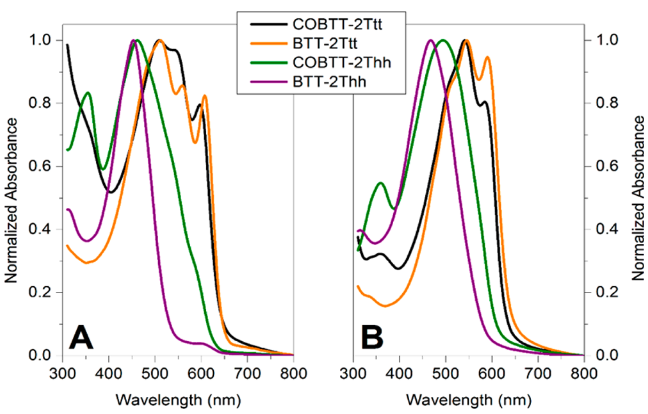

Figure 2. (A) UV–vis absorption spectra of the various **BTT** copolymers in dilute *o*-DCB solution (3 mg/L) and (B) spin-coated from *o*-DCB (5 mg/mL).

The introduction of a carbonyl group on the **BTT** moiety leads to a second absorption peak at shorter wavelengths (~350 nm), as observed in both solution and solid state UV–vis absorption spectra of **COBTT-2Thh**.[16] It also seems that the peak at around 500 nm in the solution spectrum shows weak vibronic features at lower energies, thus suggesting that the introduction of the carbonyl group on the **BTT** unit promotes aggregation in solution. This observation is further substantiated by considering the solution spectra recorded at various temperatures (Figure S1). The peak shape sharpens as a function of increasing temperature and the weak vibronic features are disappearing, hence supporting the hypothesis of an increased aggregation of **COBTT-2Thh** in solution. We speculate that this increased aggregationnal behavior of **COBTT-2Thh** is the result of dipolar intermolecular interactions originating from the carbonyl groups and leading to stronger interchain interactions compared to **BTT-2Thh**.

For the tail-to-tail coupled **BTT** polymers, the UV–vis absorption spectra are dominated by the polymers strong tendency to aggregate. The absorption spectra of both **tt** copolymers are red-shifted compared to the **hh** copolymers. This bathochromic shift finds its origin in the more planar backbone which allows a better electron delocalization along the conjugated polymer backbone and stronger $\pi-\pi$ interactions compared to the twisted head-to-head polymers. The solid state absorption spectra of both **COBTT-2Ttt** and **BTT-2Ttt** present similar vibronic features and are only slightly red-shifted compared to the solution spectra, which supports the idea of polymer aggregates in solution. To elucidate the absorption spectra of fully dissolved polymer chains, the absorption spectra were measured at different temperatures as depicted in Figure 3.

The well-defined vibronic transitions in the UV–vis spectrum of **BTT-2Ttt** at 15 °C reduce intensity at higher temperatures, revealing the hypsochromically shifted spectrum of the solvated polymer with a maximum around 470 nm (Figure 3B). In case of **COBTT-2Ttt**, the aggregation in

Table 2. Optical Properties and Energy Levels of the Different BTT Copolymers

			PESA	DFT	
polymer	λ_{max} soln[a] (nm)	λ_{max} film[b] (nm)	HOMO/LUMO[c] (eV)	HOMO/LUMO[d] (eV)	E_g^{opt}/E_g^{calc} (eV)
COBTT-2Ttt	509, 546, 597	359, 541, 583	−5.3/−3.3	−5.0/−2.8	2.0/2.2
BTT-2Ttt	511, 559, 609	545, 592	−4.8/−2.9	−4.8/−2.5	1.9/2.3
COBTT-2Thh	354, 462	360, 493	−5.4/−3.3	−5.2/−2.7	2.1/2.5
BTT-2Thh	453	467	−5.1/−2.9	−5.0/−2.4	2.2/2.6

[a]Measured in dilute *o*-dichlorobenzene solution. [b]Spin-coated from 5 mg/mL *o*-dichlorobenzene solution. [c]The LUMO energy is estimated by adding the absorption onset to the HOMO. [d]Determined by TD-DFT on the energy-minimized tetramers (B3LYP/6-31G*), alkyl chains were substituted with ethyl groups.

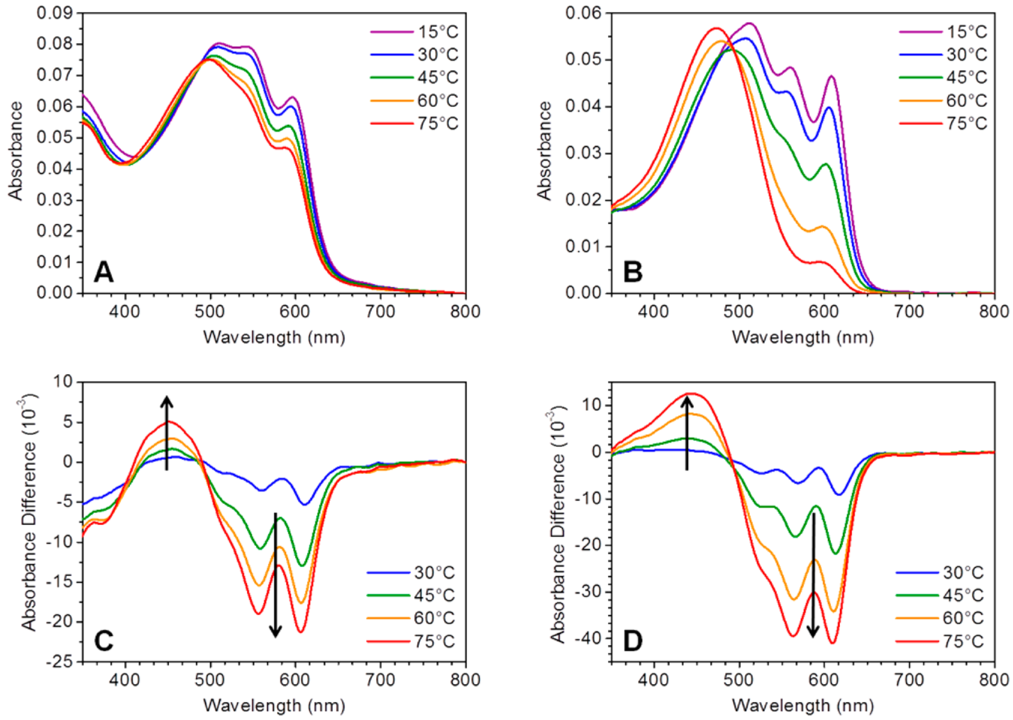

Figure 3. Temperature-dependent UV−vis absorption spectra of **COBTT-2Ttt** (A) and **BTT-2Ttt** (B) in dilute *o*-DCB solution (3 mg/L) and the corresponding difference spectra of **COBTT-2Ttt** (C) and **BTT-2Ttt** (D), respectively.

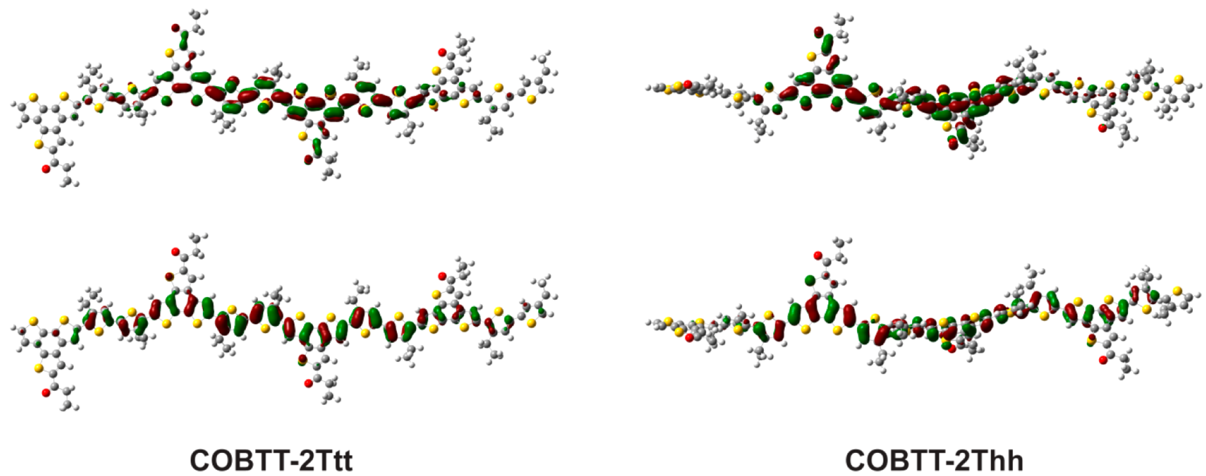

Figure 4. Graphical representation of the HOMO (bottom) and LUMO (top) of **COBTT-2Ttt** (left column) and **COBTT-2Thh** (right column).

solution seems to be much more pronounced, so that even at 75 °C the absorption spectrum is dominated by vibronic transitions. The deconvoluted absorption bands are depicted in the difference spectra shown in Figure 3C,D and stress the importance of polymer chain aggregation in solution. For both polymers the low-energy absorption bands (~550 and ~600 nm) attributed to polymer aggregates decrease with increasing temperature, and new absorption bands from fully solvated polymer chains evolve around 450 nm.

Besides the influence the alkyl chain positioning has on the absorption properties, this structural feature can also be exploited to tune the frontier energy levels (Table 2). As previously mentioned, the head−head coupling causes a backbone twist, which reduces the effective conjugation length and increases the optical bandgap. The bandgap of **BTT-2Ttt** was estimated to be 1.9 eV, and the highest occupied molecular orbital (HOMO) energy level was measured to be −4.8 eV by photoelectron spectroscopy in air. Compared to the backbone twisted **BTT-2Thh**, the tail−tail coupled polymer has a 0.3 eV higher lying HOMO energy level, resulting in a smaller bandgap than for the **BTT-2Thh** polymer because the LUMO energy levels are not affected by the alkyl chain positioning on the polymer backbone. The introduction of the electron-withdrawing carbonyl groups on the **BTT** unit lowers the LUMO energy levels of both **COBTT** polymers by 0.4 eV compared to the **BTT** polymers, but the overall bandgaps are barely affected (~2.0 eV). In addition, the alkyl chain arrangement has less of an effect on the HOMO energy levels, which have been measured to be −5.3 eV for **COBTT-2Ttt** and −5.4 eV in the case of **BTT-2Ttt**. As we have previously emphasized that the presence of carbonyl groups encourages interchain aggregation and as a consequence reduces backbone

dx.doi.org/10.1021/ma500163u | *Macromolecules* 2014, 47, 2883−2890

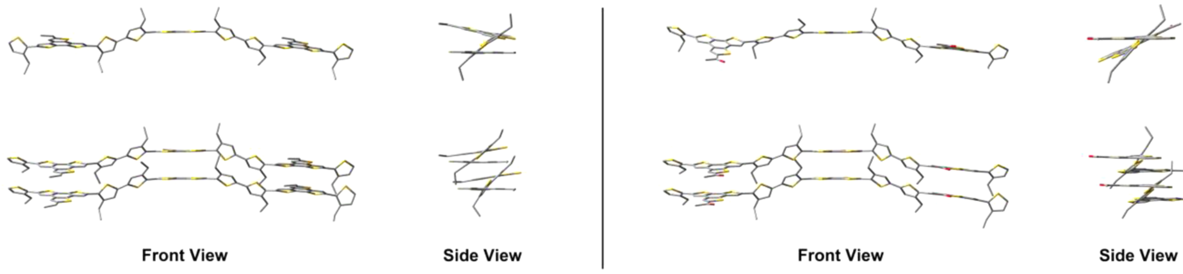

Figure 5. Optimized geometries of **BTT-2Ttt** (left) and **COBTT-2Ttt** (right) trimer and trimer stack. For clarity, all hydrogen atoms have been removed of the molecular structures.

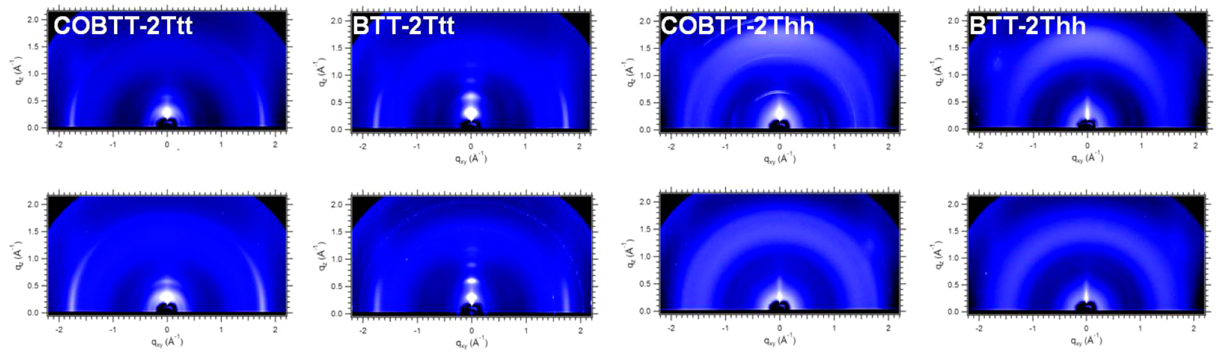

Figure 6. GIXD detector images of the various **BTT** polymers. Thin films were spin-coated from *o*-DCB solution (5 mg/mL) on Si/SiO_2 substrates: (top row) as-cast thin films and (bottom row) after annealing at 200 °C for 10 min.

twisting, therefore lowering the HOMO energy levels less than in the case of the head-to-head coupled **BTT** copolymers.

Density functional theory calculations were employed to investigate the frontier orbital wave functions distribution and how the electron-withdrawing carbonyl, the induced backbone twist, influences them. Because the calculation load increases rapidly with the number of atoms, we will focus on the optimization of tetramers with shorter ethyl side chains. Even though ethyl side chains are much shorter than hexyl or hexadecyl ones, they will allow us nevertheless to model the steric hindrance at reasonable computational costs.

The optimized ground state geometry of the tetramers was calculated using the B3LYP hybrid functional and the 6-31G* basis set.[17] The HOMO and LUMO wave function distributions of both **COBTT-2T** isomers are shown in Figure 4. In the case of **COBTT-2Ttt** the tetramer adopts a nearly coplanar geometry with small torsional angles of 6° between the two alkylthiophene units. This allows both HOMO and LUMO to be fully delocalized along the conjugated backbone, contrary to the **COBTT-2Thh** tetramer. On the basis of the blue-shifted UV−vis spectra, one could expect a significantly reduced conjugation pathway and the DFT calculations confirm this assumption. A large torsional angle of ~70° was measured between the alkylthiophene moieties in the optimized tetramers. This significant torsion of the backbone causes both HOMO and LUMO to be significantly distorted around the bithienyl system. Even though the wave functions are still somehow delocalized over the backbone, they seem to be more localized on the chain segments separated by these large torsional angles. By comparing the **hh** isomer to the **tt** one, it is apparent that especially the LUMO distribution on the **COBTT** unit is more pronounced in the case of the **COBTT-2Thh** than for **COBTT-2Ttt**. A similar, but less important, effect is observed for the HOMO distribution, thus confirming that the effective conjugation length is significantly reduced by the introduced backbone twists. The **BTT-2T** tetramers behave in a very similar way (Figures S2 and S3) with regard to the wave function distribution, but the backbone twist in the **BTT-2Thh** tetramer does not seem to affect the intensities of the wave functions on the **BTT** chromophore. This observation might be in relation with the lack of the carbonyl group next to the **BTT** ring system, which has been shown previously to disturb the electron distribution in the π-conjugated **BTT** system.[16]

Based on the UV−vis absorption studies discussed above and the differences in torsional angles between the different polymers, it has to be assumed that the polymers aggregate differently. Geometrical optimization calculations were performed on an isolated trimer and a trimer stack to gain some insight into how the torsional angles between repeating units are influenced by interchain aggregation. To accommodate the long-range $\pi-\pi$ interactions in the geometry optimization of the trimer stack, the ωB97XD functional with the SVP basis set was employed.[18,19] As the aggregation is playing a more important role in the coplanar **tt** coupled polymers, we limited our calculations on the study of **BTT-2Ttt** and **COBTT-2Ttt** (Figure 5).

As evidenced from the optimized geometries in Figure 5, it is apparent that both polymers undergo strong intermolecular interactions, which should be beneficial with regard to charge transport. The torsional angle (~44°) between the **BTT** core and the **2T** system remains nearly unchanged between the isolated trimer and the trimer stack in **BTT-2Ttt**. However, in the case of the **COBTT-2Ttt** polymer the torsional angle is decreased by 7° to 43°, when the isolated trimer is introduced into the stacked system. This indicates the importance of the solubilizing alkyl chain placement and its influence on the polymer chain conformation cannot be neglected. In addition,

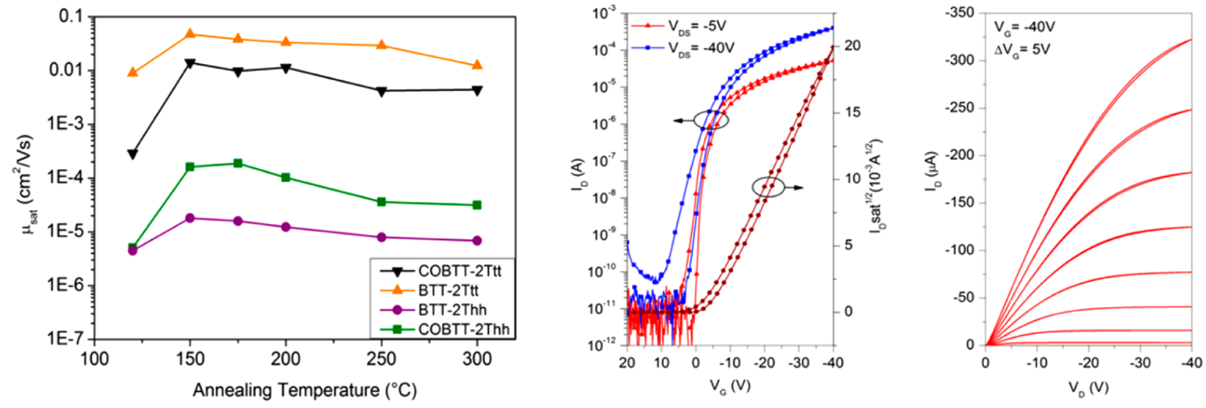

Figure 7. (left) Graphical representation of the saturated hole mobility as a function of annealing temperature. (middle) Transfer curves and (right) output characteristics of **BTT-2Ttt**.

the **BTT** chromophores seem to undergo close π-stacking interactions (~3.5 Å) in both polymers, which should promote intermolecular charge hopping and molecular order in the solid state.

Despite the intense aggregation observed for the **tt** coupled polymers in UV–vis studies, differential scanning calorimetry (DSC) showed only minor signs of crystallinity for the different **BTT** polymers (Figure S4). Only for **BTT-2Ttt** phase transitions were observed in the temperature range from 0 to 300 °C, whereas all other polymer samples were featureless in this temperature range. According to the first heating and cooling cycles, a broad and partially reversible transition is observed at around 280 °C for **BTT-2Ttt**. The **hh** coupled **BTT** polymers did not show any transitions, which was anticipated given the backbone twist which should hinder crystallinity and long-range order. To further investigate the molecular packing of the materials, grazing-incidence X-ray diffraction (GIXD) studies were carried out and the 2D images are presented in Figure 6.

The most significant differences between the **hh** and **tt** isomers are the scattering intensities, which have been found to be more intense in the case of the **tt** isomers. Additionally the **hh** polymers prefer a face-on orientation on the substrate, whereas the **tt** polymers orient normal to the plane of the substrate (edge-on). Two orders of (h00) scatterings are observed in the as-cast film of **COBTT-2Ttt**. Upon annealing the scattering intensity increases, but the lamellar sheets remain poorly aligned with respect to the substrate as evidenced by the observed arching. The crystallites of **BTT-2Ttt** are much more oriented both in the out-of-plane and in-plane direction. Upon thermal annealing the out-of-plane scattering intensifies, whereas the in-plane scattering sharpens. **BTT-2Ttt** adopts a highly ordered lamellar packing with short π–π stacking distances, similar to **P3HT**.[20] This is in excellent agreement with the DSC measurements, confirming the more semicrystalline nature of **BTT-2Ttt** compared to **COBTT-2Ttt**.

Weaker scattering is observed for both **COBTT-2Thh** and **BTT-2Thh** polymers compared to the aforementioned **tt** coupled polymers, suggesting that the conformational disorder introduced by the **hh** coupling prevents the material from adopting any long-range order in the solid state.

To evaluate the potential of the new **BTT** polymers as semiconductors, organic field effect transistors were fabricated. In a first attempt, bottom gate–bottom contact (BGBC) devices on hexamethyldisilazane (HMDS) treated SiO_2 substrates with gold electrodes were fabricated. Because of the challenging solubility of the **tt** coupled polymers, the semiconducting layers were processed from 1,2,4-trichlorobenzene (TCB) and subsequently annealed at elevated temperatures. In Figure 7, the saturated hole mobility is plotted as a function of annealing temperature. Maximum mobilities were achieved at annealing temperatures around 175 °C. On the one hand, the high annealing temperatures help remove residual TCB (bp = 214 °C) from the thin film and at the same time the film crystallinity increased as previously determined by the GIXD measurements. The highest hole mobility (0.04 cm^2/(V s)) was achieved with the **BTT-2Ttt** polymer with a low threshold voltage of −0.5 V and minor hysteresis, as seen in the transfer curves in Figure 7. The hole mobility of **COBTT-2Ttt** was only marginally lower, at 0.01 cm^2/(V s), but the threshold voltage increased to −8.9 V. The increase in threshold voltage is likely to be linked to an increased number of traps in the polymer film, as the extremely high tendency of **COBTT-2Ttt** to aggregate made it difficult to purify the polymer accordingly. The charge carrier mobilities dropped significantly for both **hh** coupled **BTT** polymers (Table 3), of which the detailed device characteristics can be found in the Supporting Information (Figure S5).

Table 3. OFET Device (BGBC, HMDS Treated SiO_2 Substrate) Characteristics of the Different BTT Copolymers

polymer	μ_{sat} (cm^2/(V s))	V_T (V)	I_{on}/I_{off}
COBTT-2Ttt	0.01	−8.9	~10^6
BTT-2Ttt	0.04	−0.5	~10^7
COBTT-2Thh	1.2×10^{-3}	−12	~10^4
BTT-2Thh	1.6×10^{-5}	−17	~10^3

Thermal annealing increases the hole mobilities of all devices by 1 order of magnitude. To get a better understanding of why the mobilities increase and how the film morphologies of the various **BTT** polymers are affected, atomic force microscopy (AFM) experiments were carried out on as-cast and thermally annealed thin polymer films (Figure 8). The **tt** coupled polymers have rougher surfaces than their **hh** coupled counterparts, which is most likely related to the poorer solubility and higher tendency of **COBTT-2Ttt** and **BTT-2Ttt** to aggregate. The highly soluble head-to-head coupled polymers form very smooth and homogeneous films with root-mean-squared (RMS) roughnesses not exceeding 0.25 nm in the as-cast films. Thermal annealing of the films at 175 °C

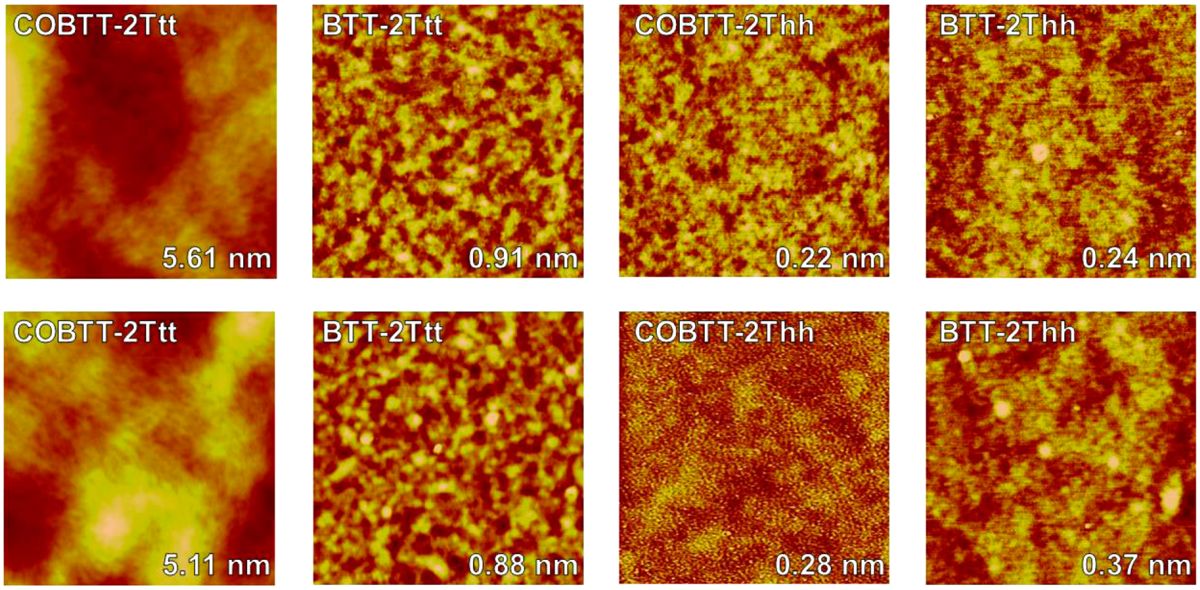

Figure 8. 2×2 μm AFM micrographs (tapping-mode) of as-cast (top row) and annealed (bottom row) **BTT** polymer films. The root-mean-squared roughness of each film is indicated in nm.

only marginally influences the surface roughness, but the overall morphologies of both **COBTT** polymer thin films are modified as evidenced by the phase images (Figures S6−S13). These morphological changes are likely to be related to the more efficient solvent removal at higher annealing temperature. Before thermal annealing the phase image of **COBTT-2Ttt** shows the presence of randomly oriented short needle-like structures; however, upon annealing these structures are transformed into longer more oriented polymer fibrils. The best performing **BTT-2Ttt** polymer forms smoother films than the aforementioned **COBTT-2Ttt** polymer, and its morphology strongly resembles the ones of both head-to-head coupled polymers. Nevertheless, there are subtle differences between those morphologies. **BTT-2Ttt** shows larger domain sizes and consequently less grain boundaries, which correlates well with the higher hole mobility. The **COBTT-2Thh** film, on the other hand, presents larger domains at the surface prior to thermal annealing but smaller, homogeneously dispersed domains after annealing at 175 °C for 10 min. The presence of a multitude of smaller domains could result potentially in more grain boundaries, which was shown in the past to hinder charge transport due to improved charge trapping.[21] The exact origin of these morphological changes are not yet understood but nevertheless highlight the importance of the alkyl chain placement along the polymer backbone and the significant effects this subtle structural change can have on the film morphology.

One of the aims of this work was to increase ambient stability of the **BTT** polymers by introducing electron-withdrawing carbonyl groups onto the conjugated backbone. To verify the effectiveness of this approach, the BGBC transistor devices were removed from the protective atmosphere of the glovebox and exposed to ambient conditions (Figure 9). No significant changes in saturated hole mobilities could be observed, suggesting that all polymers are intrinsically stable under ambient operating conditions within the tested time scale.

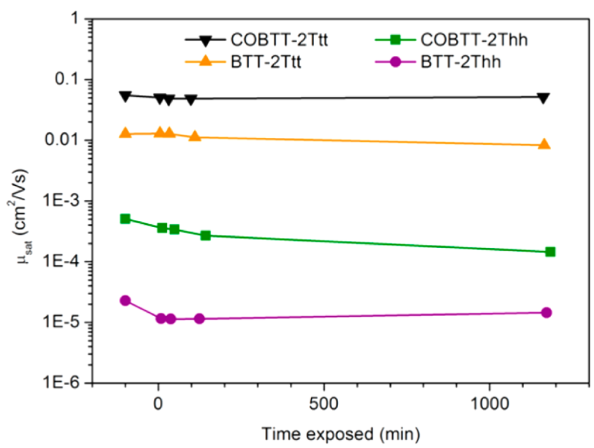

Figure 9. Ambient stability of BGBC devices; negative *x* values refer to saturated hole mobilities tested under a nitrogen atmosphere.

■ CONCLUSION

We synthesized and characterized four new benzotrithiophene-containing polymers, and by altering the solubilizing alkyl chain nature and positioning, we were able to not only influence the frontier energy levels but also the polymer's solubility and solid state packing. The steric hindrance along the polymer backbone could be reduced by copolymerizing the **BTT** unit with 5,5′-dihexyl-2,2′-bithiophene, leading to strong aggregation, in both solution and solid state. The enhanced order of **COBTT-2Ttt** and **BTT-2Ttt**, evidenced by GIXD measurements is also believed to be at the origin of the higher hole mobilities (up to 0.1 cm^2/(V s)) observed in BGBC thin film transistors compared to the head-to-head coupled polymers. Copolymerizing the **BTT** units with the head-to-head coupled 3,3′-dihexyl-2,2′-bithiophene introduces significant torsional angles along the polymer backbone, which on the one hand increases the polymers processability but on the other hand prevents the polymer chains from ordering in the solid state. The large torsional angles were found to significantly disturb the conjugation along the backbone, which lead to much lower hole mobilities ($<10^{-3}$ $cm^2/(V\ s)$) in OFET.

■ ASSOCIATED CENTENT

Ⓢ Supporting Information

Synthetic procedures, graphical representations of **BTT-2T** frontier energy levels, OFET transfer and output curves, temperature-dependent UV–vis absorption spectra, polymer DSC, and AFM images. This material is available free of charge via the Internet at http://pubs.acs.org.

■ AUTHOR INFORMATION

Corresponding Author

*E-mail b.schroeder10@imperial.ac.uk (B.C.S.).

Notes

The authors declare no competing financial interest.

■ ACKNOWLEDGMENTS

The authors acknowledge the Imperial College High Performance Computing Service for providing the computing facilities to perform the quantum-mechanical calculations and Dr. Alexandra Simperler from NSCCS for helpful discussions and suggestions with the quantum chemical calculations. This work was in part carried out under the EPSRC Project EP/F056710/1 and EP/G037515/1 with support from the Centre for Plastic Electronics at Imperial College London and the National Research Fund of Luxembourg. Portions of this research were carried out at the Stanford Synchrotron Radiation Lightsource, a Directorate of SLAC National Accelerator Laboratory and an Office of Science User Facility operated for the U.S. Department of Energy Office of Science by Stanford University.[22]

■ REFERENCES

(1) So, F. *Organic Electronics: Materials, Processing, Devices and Applications*; CRC Press: Boca Raton, FL, 2010.

(2) Holliday, S.; Donaghey, J. E.; McCulloch, I. *Chem. Mater.* **2013**, *26*, 647.

(3) Mei, J.; Bao, Z. *Chem. Mater.* **2013**, *26*, 604.

(4) Bobbert, P. A.; Sharma, A.; Mathijssen, S. G. J.; Kemerink, M.; de Leeuw, D. M. *Adv. Mater.* **2012**, *24*, 1146.

(5) Biniek, L.; Schroeder, B. C.; Nielsen, C. B.; McCulloch, I. *J. Mater. Chem.* **2012**, *22*, 14803.

(6) Rieger, R.; Beckmann, D.; Mavrinskiy, A.; Kastler, M.; Müllen, K. *Chem. Mater.* **2010**, *22*, 5314.

(7) Kim, J.; Lim, B.; Baeg, K.-J.; Noh, Y.-Y.; Khim, D.; Jeong, H.-G.; Yun, J.-M.; Kim, D.-Y. *Chem. Mater.* **2011**, *23*, 4663.

(8) Ko, S.; Verploegen, E.; Hong, S.; Mondal, R.; Hoke, E. T.; Toney, M. F.; McGehee, M. D.; Bao, Z. *J. Am. Chem. Soc.* **2011**, *133*, 16722.

(9) Nielsen, C. B.; McCulloch, I. *Prog. Polym. Sci.* **2013**, *38*, 2053.

(10) Nielsen, C. B.; Fraser, J. M.; Schroeder, B. C.; Du, J.; White, A. J. P.; Zhang, W.; McCulloch, I. *Org. Lett.* **2011**, *13*, 2414.

(11) Schroeder, B. C.; Nielsen, C. B.; Kim, Y. J.; Smith, J.; Huang, Z.; Durrant, J.; Watkins, S. E.; Song, K.; Anthopoulos, T. D.; McCulloch, I. *Chem. Mater.* **2011**, *23*, 4025.

(12) Biniek, L.; Fall, S.; Chochos, C. L.; Anokhin, D. V.; Ivanov, D. A.; Leclerc, N.; Lévêque, P.; Heiser, T. *Macromolecules* **2010**, *43*, 9779.

(13) Yasuda, T.; Sakai, Y.; Aramaki, S.; Yamamoto, T. *Chem. Mater.* **2005**, *17*, 6060.

(14) Kim, Y.; Cook, S.; Kirkpatrick, J.; Nelson, J.; Durrant, J. R.; Bradley, D. D. C.; Giles, M.; Heeney, M.; Hamilton, R.; McCulloch, I. *J. Phys. Chem. C* **2007**, *111*, 8137.

(15) Nielsen, K. T.; Bechgaard, K.; Krebs, F. C. *Macromolecules* **2005**, *38*, 658.

(16) Nielsen, C. B.; Sohn, E.-H.; Cho, D.-J.; Schroeder, B. C.; Smith, J.; Lee, M.; Anthopoulos, T. D.; Song, K.; McCulloch, I. *ACS Appl. Mater. Interfaces* **2013**, *5*, 1806.

(17) Gaussian 09: Frisch, M. J.; Trucks, G. W.; Schlegel, H. B.; Scuseria, G. E.; Robb, M. A.; Cheeseman, J. R.; Scalmani, G.; Barone, V.; Mennucci, B.; Petersson, G. A.; Nakatsuji, H.; Caricato, M.; Li, X.; Hratchian, H. P.; Izmaylov, A. F.; Bloino, J.; Zheng, G.; Sonnenberg, J. L.; Hada, M.; Ehara, M.; Toyota, K.; Fukuda, R.; Hasegawa, J.; Ishida, M.; Nakajima, T.; Honda, Y.; Kitao, O.; Nakai, H.; Vreven, T.; Montgomery, J. A., Jr.; Peralta, J. E.; Ogliaro, F.; Bearpark, M.; Heyd, J. J.; Brothers, E.; Kudin, K. N.; Staroverov, V. N.; Kobayashi, R.; Normand, J.; Raghavachari, K.; Rendell, A.; Burant, J. C.; Iyengar, S. S.; Tomasi, J.; Cossi, M.; Rega, N.; Millam, J. M.; Klene, M.; Knox, J. E.; Cross, J. B.; Bakken, V.; Adamo, C.; Jaramillo, J.; Gomperts, R.; Stratmann, R. E.; Yazyev, O.; Austin, A. J.; Cammi, R.; Pomelli, C.; Ochterski, J. W.; Martin, R. L.; Morokuma, K.; Zakrzewski, V. G.; Voth, G. A.; Salvador, P.; Dannenberg, J. J.; Dapprich, S.; Daniels, A. D.; Farkas, Ö.; Foresman, J. B.; Ortiz, J. V.; Cioslowski, J.; Fox, D. J. Gaussian, Inc.: Wallingford, CT, 2009.

(18) Chai, J.-D.; Head-Gordon, M. *Phys. Chem. Chem. Phys.* **2008**, *10*, 6615.

(19) Schäfer, A.; Horn, H.; Ahlrichs, R. *J. Chem. Phys.* **1992**, *97*, 2571.

(20) Kline, R. J.; DeLongchamp, D. M.; Fischer, D. A.; Lin, E. K.; Richter, L. J.; Chabinyc, M. L.; Toney, M. F.; Heeney, M.; McCulloch, I. *Macromolecules* **2007**, *40*, 7960.

(21) Jimison, L. H.; Toney, M. F.; McCulloch, I.; Heeney, M.; Salleo, A. *Adv. Mater.* **2009**, *21*, 1568.

(22) Certain commercial equipment, instruments, or materials are identified in this paper in order to specify the experimental procedure adequately. Such identification is not intended to imply recommendation or endorsement by the National Institute of Standards and Technology, nor is it intended to imply that the materials or equipment identified are necessarily the best available for the purpose.